Constraining U.S. ammonia emissions using TES remote sensing observations and the GEOS-Chem adjoint model

L. Zhu,[1] D. K. Henze,[1] K. E. Cady-Pereira,[2] M. W. Shephard,[3,4] M. Luo,[5]
R. W. Pinder,[6] J. O. Bash,[6] and G.-R. Jeong[1,6]

Received 2 August 2012; revised 25 December 2012; accepted 3 January 2013.

[1] Ammonia (NH_3) has significant impacts on biodiversity, eutrophication, and acidification. Widespread uncertainty in the magnitude and seasonality of NH_3 emissions hinders efforts to address these issues. In this work, we constrain U.S. NH_3 sources using observations from the TES satellite instrument with the GEOS-Chem model and its adjoint. The inversion framework is first validated using simulated observations. We then assimilate TES observations for April, July, and October of 2006 through 2009. The adjoint-based inversion allows emissions to be adjusted heterogeneously; they are found to increase in California throughout the year, increase in different regions of the West depending upon season, and exhibit smaller increases and occasional decreases in the Eastern U.S. Evaluations of the inversion using independent surface measurements show reduced model underestimates of surface NH_3 and wet deposited NH_x in April and October; however, the constrained simulation in July leads to overestimates of these quantities, while TES observations are still under predicted. Modeled sulfate and nitrate aerosols concentrations do not change significantly, and persistent nitrate overestimation is noted, consistent with previous studies. Overall, while satellite-based constraints on NH_3 emissions improve model simulations in several aspects, additional assessment at higher horizontal resolution of spatial sampling bias, nitric acid formation, and diurnal variability and bi-directionality of NH_3 sources may be necessary to enhance year-round model performance across the full range of gas and aerosol evaluations.

Citation: Zhu, L., D. K. Henze, K. E. Cady-Pereira, M. W. Shephard, M. Luo, R. W. Pinder, J. O. Bash, and G.-R. Jeong (2013), Constraining U.S. ammonia emissions using TES remote sensing observations and the GEOS-Chem adjoint model, *J. Geophys. Res. Atmos.*, *118*, doi:10.1002/jgrd.50166.

1. Introduction

[2] Emissions of ammonia (NH_3) from anthropogenic sources pose several environmental concerns. Ammonia affects air quality and climate through its role in the mass, composition, and physical properties of tropospheric aerosol. Ammonium nitrate and ammonium sulfate make up a substantial fraction of atmospheric fine particulate matter ($PM_{2.5}$), exposure to which has been statistically associated with inhibited lung development, cardiovascular diseases, and premature mortality [*Pope et al*., 2002; *Schwartz et al*., 2002; *Reiss et al*., 2007]. These fine particulates ($PM_{2.5}$) also contribute to haze and thus impact visibility. Further, when deposited in excess, reactive nitrogen, including ammonia, can cause detrimental nutrient imbalances to sensitive ecosystems [*Rodhe et al*., 2002; *Rabalais*, 2002].

[3] Despite the recognized importance of NH_3 emissions in the U.S. [*Aneja et al*., 2008], knowledge of their magnitude is severely limited; NH_3 emissions are primarily from agricultural sources whose strengths are difficult to characterize. Uncertainty in NH_3 undermines efforts to understand historical and present levels of $PM_{2.5}$ [*Yu et al.*, 2005; *Nowak et al*., 2006; *Zhang et al*., 2008; *Wu et al*., 2008; *Stephen and Aneja*, 2008; *Beusen et al*., 2008; *Simon et al*., 2008; *Henze et al*., 2009] and hinders estimates of the response of $PM_{2.5}$ to control measures because of the key role that NH_3 plays in governing the balance of inorganic fine particulate species [*Dennis et al*., 2008]. Model estimates of inorganic $PM_{2.5}$ have been compared to surface measurements [*Park et al*., 2004, 2006; *Liao et al*., 2007; *Henze et al*., 2009; *Pye et al*., 2009;

All supporting information may be found in the online version of this article.

[1]Department of Mechanical Engineering, University of Colorado, Boulder, Colorado, USA.
[2]Atmospheric and Environmental Research, Inc., Lexington, Massachusetts, USA.
[3]Atmospheric and Climate Application, Inc., East Gwillimbury, Ontario, Canada.
[4]Environment Canada, Toronto, Ontario, Canada.
[5]Jet Propulsion Laboratory, California Institute of Technology, Pasadena, California, USA.
[6]US Environmental Protection Agency, Research Triangle Park, North Carolina, USA.

Corresponding author: D. K. Henze, Department of Mechanical Engineering, University of Colorado, Boulder, CO, USA. (daven.henze@colorado.edu)

2169-897X/13/10.1002/jgrd.50166

Heald et al., 2012] and measurements from aircraft campaigns [*Heald et al*., 2005, 2006]; NH_3 emissions are frequently indicated to be a likely cause of discrepancies. On a larger scale, NH_3 emissions rates are a critical source of uncertainty in global budgets of the atmospheric transport and deposition of reactive nitrogen [*Sutton et al*., 2007; *Galloway et al*., 2008; *Schlesinger*, 2009].

[4] These are several reasons for the persistence of uncertainties in NH_3 inventories. Characterizing NH_3 sources from the bottom up requires spatially and temporally resolved data such as detailed farming practices and intensity. These data are rarely available nationally as direct measurements of NH_3 emissions at such scales are prohibitive owing to cost. Therefore, top-down approaches have become an attractive option for providing additional constraints. While direct observations of gas-phase NH_3 do exist in select locations, observations of other chemically related species are much more prevalent. Furthermore, NH_3 can rapidly partition to form aerosol ammonium (NH_4^+) which can limit the utility of gas-phase observations alone.

[5] Consequently, owing to the paucity of direct observations of NH_3 and the difficulty of constraining the NH_x (=NH_3 + NH_4^+) system, measurements of species that are regulated by the amount of available NH_3 have been looked to for constraints on estimates of NH_3 emissions. The National Emissions Inventory (NEI) for NH_3 is coarsely constrained by top-down estimates from the inverse modeling studies of *Gilliland et al*. [2003, 2006]. Measurements of wet deposited NH_x were used as constraints, because wet deposited NH_x estimates depend less than NH_3 on model sensitivity to aerosol partitioning. A drawback to this approach is the sensitivity to the precipitation fields in the meteorological re-analysis data driving the chemical transport model and to the parameterization of NH_x wet scavenging, both of which are aspects that are difficult to model accurately and hinder the inversion during some seasons. Taking an alternate approach, *Henze et al*. [2009] used surface measurements of SO_4^{2-} and NO_3^- from the IMPROVE network to constrain the amount of NH_3 partitioned into the aerosol phase as NH_4^+ (which is strongly coupled to SO_4^{2-} and NO_3^-). In this way, aerosol-phase observations were used to constrain NH_3 concentrations and, hence, NH_3 emissions. This approach, however, is sensitive to model bias in HNO_3, which may be significant [*Zhang et al*., 2012; *Heald et al*., 2012].

[6] Despite these recent efforts, comparisons of inverse modeling results to the bottom-up NH_3 inventory of *Pinder et al*. [2006] show that considerable disagreements remain in the spatial and seasonal distribution of NH_3 emissions throughout the U.S. [*Henze et al*., 2009]; at odds are estimates of the relative magnitude of spring versus summer emissions. A limiting factor in reconciling these differences is infrequent and sparse in situ observations, even for the aerosol-phase measurements, and a shortage of direct constraints on gas-phase NH_3. Without understanding the NH_x system as a whole, and without tools to link observations of these species over the continent to emissions, studies of NH_3 or NH_4^+ alone may suffer in terms of utility for constraining emissions inventories at a national scale [*Pinder et al*., 2006].

[7] The detection of boundary layer ammonia from space [*Beer et al*., 2008; *Clarisse et al*., 2009, 2010; *Shephard et al*., 2011] provides a new opportunity for reducing persistent uncertainties in our understanding of the distribution and impacts of atmospheric ammonia. Initial comparisons to global model NH_3 distributions indicate that NH_3 sources may be widely underestimated [*Clarisse et al*., 2009; *Shephard et al*., 2011]. *Pinder et al*. [2011] have verified the utility of such measurements for tracking observed spatial and temporal trends in surface level NH_3 concentrations. Subsequent studies indicate that underestimates of NH_3 sources exist in California and throughout the U.S. in the spring [*Nowak et al*., 2012; *Walker et al*., 2012; *Heald et al*., 2012]. Therefore, we consider here how inverse modeling with assimilation of satellite observations of NH_3 can be used to further provide constraints on NH_3 sources. Section 2 describes the models and inverse methodology used in this study. We then present details of the remote sensing observations (Section 3), followed by inverse modeling tests using simulated observations (Section 4) and real observations (Section 5). Finally, we evaluate the model results by comparing them to independent data sets omitted from the inversion (Section 6) and present our conclusions (Section 7).

2. Methods

2.1. GEOS-Chem

[8] GEOS-Chem is a chemical transport model driven with assimilated meteorology from the Goddard Earth Observing System (GEOS) of the NASA Global Modeling and Assimilation Office [*Bey et al*., 2001]. The tropospheric oxidant chemistry simulation in GEOS-Chem includes a detailed ozone-NO_x-hydrocarbon chemical mechanism of 80 species and over 300 reactions [*Bey et al*., 2001]. GEOS-Chem includes an online secondary inorganic aerosol simulation introduced and described in full by *Park et al*. [2004]. Global anthropogenic sources and natural sources of NH_3 are from the 1990 GEIA inventory [*Bouwman et al*., 1997]. Over the U.S., anthropogenic NH_3 emissions are taken from the 2005 U.S. National Emissions Inventory (NEI), with seasonality as described in *Park et al*. [2004], and the CAC inventory for Canada [*van Donkelaar et al*., 2008]. Biomass burning emissions are from *van der Werf et al*. [2006], and biofuel emissions are from *Yevich and Logan* [2003]. The total U.S. and global NH_3 emissions both before and after the optimization are shown in Table 1.

Table 1. Total U.S. and Global NH_3 Emissions Before and After Optimization.

Simulation	U.S. (Gg/month)	Global (Tg/month)
April		
Initial	234	5.67
Optimized	424	6.03
July		
Initial	509	6.37
Optimized	799	6.76
October		
Initial	272	5.69
Optimized	362	5.80

2.2. GEOS-Chem Adjoint Model

[9] The adjoint model is an efficient tool for calculating the gradient of a scalar model response function with respect to all model parameters simultaneously. The adjoint of the GEOS-Chem model was developed specifically for inverse modeling of precursors of inorganic $PM_{2.5}$ with explicit inclusion of gas-phase chemistry, heterogeneous chemistry, and treatment of the thermodynamic couplings of the sulfate-ammonium-nitrate-water aerosol system [*Henze et al*., 2007, 2009]. As the only adjoint model to explicitly represent this system, it is uniquely capable of assimilating speciated measurements of both gaseous and particulate components using the 4D-Var method [*Sandu et al*., 2005]. The accuracy of the adjoint model calculations is verified through extensive comparisons of adjoint to finite difference sensitivities. In order to maximize points of comparison between these two approaches, we consider both ensembles of 1-D models (i.e., no horizontal transport) as well as spot tests of the full 3-D adjoint model (testing the full adjoint model for each parameter is prohibitively time consuming, as it would require separate forward model calculations for each of the approximately 10^5 parameters). Figure 1 shows the results of a week-long test of the sensitivity of surface level NH_3 concentrations in each model column to NH_3 emissions in that column. Sensitivities calculated using the adjoint model are compared with sensitivities calculated using finite differences. All points lie along or near the 1:1 line, demonstrating the accuracy of the adjoint model. Further validation of the adjoint model can be found in previous papers [*Henze et al*., 2007, 2009, 2012].

2.3. Inverse Modeling

[10] Data assimilation techniques provide a framework for combining observations and models to form an optimal estimation of the state of a system, which in this case is the chemical makeup of the troposphere. To start with, a range of parameters are constructed using control variables, $\boldsymbol{\sigma}$, to adjust elements of the vector of model parameters, $\mathbf{p}$, via application as scaling factors, $p = p_a e^{\sigma}$, where $\mathbf{p}_a$ is the prior parameter estimate. The approach we consider iteratively employs the adjoint of an air quality model

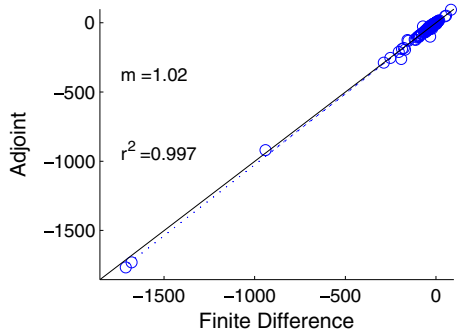

Figure 1. Validation of adjoint model sensitivities via comparison to finite difference (FD) results for week-long simulations. Shown here are the sensitivities [kg] of surface level NH_3 concentrations with respect to NH_3 emissions in an ensemble of column model simulations. Solid lines are 1:1, and dashed lines are regressions with given R^2 and slope m.

in a method referred to as 4D-Var, used here for inverse modeling of emissions. The advantage of this method is that numerous ($\mathcal{O}(10^5)$) model parameters can be optimized simultaneously while still retaining the constraints of the full forward model physics and chemistry. This approach to inverse modeling seeks $\boldsymbol{\sigma}$ that minimizes the cost function, $\mathcal{J}$, given by

$$\mathcal{J} = \frac{1}{2}\sum_{\mathbf{c}\in\Omega}(H\mathbf{c}-(\mathbf{c}_{obs}-\mathbf{b}))^T\mathbf{S}_{obs}^{-1}(H\mathbf{c}-(\mathbf{c}_{obs}-\mathbf{b})) + \frac{1}{2}\gamma(\boldsymbol{\sigma}-\boldsymbol{\sigma}_a)^T\mathbf{S}_a^{-1}(\boldsymbol{\sigma}-\boldsymbol{\sigma}_a) \quad (1)$$

where H is the observation operator, γ is the regularization parameter, $\boldsymbol{\sigma}_a$ is the prior estimate of the control variables, $\mathbf{S}_a$ and $\mathbf{S}_{obs}$ are error covariance estimates of the control variables and observations, respectively, Ω is the domain over which observations, $\mathbf{c}_{obs}$, and model predictions are available, and $\mathbf{b}$ is a bias correction explained in section 5. Overall, the cost function is a specific model response functional, the minimum value of which balances the objectives of improving model performance while ensuring the model itself remains within a reasonable range (as dictated by $\mathbf{S}_a^{-1}$) of the initial model. Gradients of the cost function with respect to the scaling factors calculated with the adjoint model, $\nabla_\sigma\mathcal{J}$, are supplied to an optimization routine (the quasi-Newton L-BFGS-B optimization routine) [*Byrd et al*., 1995; *Zhu et al*., 1994], and the minimum of the cost function is sought iteratively. At each iteration, improved estimates of the model parameters are updated and the forward model solution is recalculated.

3. Observations

3.1. Remotely Sensed NH_3 Observations From TES

[11] The high spectral resolution and good signal-to-noise ratio of the TES instrument [*Shephard et al*., 2008] enabled the first detection of tropospheric ammonia from space with measurements over Southern California and China [*Beer et al*., 2008]. TES is an infrared Fourier transform spectrometer with spectral resolution of 0.06 cm^{-1} aboard the NASA Aura satellite, launched 15 July 2004, with a local overpass time of 13:30 and 01:30 [*Schoeberl et al*., 2006]. TES global survey observations repeat with a 16 day cycle and have a nadir footprint of 5 km × 8 km, for example, that leads to about ∼180 daytime retrievals a month over North America after cloud screening (optical depths < 1.0) and applying the TES retrieval quality control flags.

[12] Comparison of model estimates to satellite observations is done via application of the following formula for the TES observational operator, H:

$$H\mathbf{c} = \mathbf{c}_a + \mathbf{A}(\mathbf{M}\mathbf{c} - \mathbf{c}_a) \quad (2)$$

where $\mathbf{c}$ is the model estimated NH_3 profile, $\mathbf{M}$ is a matrix that maps these values to the retrieval units and vertical levels, $\mathbf{A}$ is the averaging kernel, and $\mathbf{c}_a$ is the a priori NH_3 profile used for the retrieval [*Shephard et al*., 2011]. By comparing TES NH_3 profiles to mapped model estimates, $H\mathbf{c}$, rather than the native model NH_3 profile, $\mathbf{c}$, the contribution of error in $\mathbf{c}_a$ to the measurement error, $\mathbf{S}_{obs}$, is minimized [Rodgers, 2000].

[13] For the sake of 2-D visualization, the Representative Volume Mixing Ratio (RVMR) metric [*Payne et al*., 2009; *Shephard et al*., 2011] is used to provide a means of comparing TES profiles to model estimates in a manner that accounts for heterogeneity in the instrument's sensitivity to NH_3. RVMR is the average volume mixing ratio within the boundary layer, weighted by a function derived from the retrieval's averaging kernel. This represents a TES sensitivity weighted boundary layer averaged value with the influence of a priori reduced as much as possible [*Shephard et al*., 2011]. We calculate RVMR only for retrievals that have signal to noise greater than 1 and high thermal contrast. The RVMR is also calculated for the model in those locations which have valid TES retrievals.

3.2. Surface Measurements

[14] In this study, model estimates are evaluated using surface observations of NH_3, sulfate, nitrate, ammonium, and wet deposited NH_x from several monitoring networks throughout the U.S. Surface NH_3 observations are from the National Atmospheric Deposition Program (NADP) Ammonia Monitoring Network (AMoN), which is comprised of triplicate passive ammonia monitoring samplers located at 21 sites across the U.S. with a 2 week long sample accumulation [*Puchalski et al*., 2011]. All 2 week long observations in each month are averaged to give monthly concentration. The locations of these 21 monitoring stations are shown in Figure 2. Observations from each site are compared with modeled concentrations during the November 2007 through June 2010 period.

[15] Hourly surface NH_3 observations in July of 2008 are from the Southeastern Aerosol Research and Characterization (SEARCH) network [*Hansen et al*., 2003], which has monitoring stations throughout the Southeast U.S. Different sample frequencies (e.g., daily, 3 day, 6 day, 1 min, 5 min, hourly) are available at different monitoring station. Five minute long observations are available in three stations: Oak Grove, MS; Jefferson Street, GA; and Yorkville, GA. The hourly NH_3 concentration used here is the average of all 5 min long observations of these three stations in each hour.

[16] Wet deposition observations are taken from the NADP National Trends Network (NTN) (http://nadp.sws.uiuc.edu/NADP), which are predominantly located away from urban areas and point sources of pollution. NTN has more than 200 sites with week-long sample accumulation.

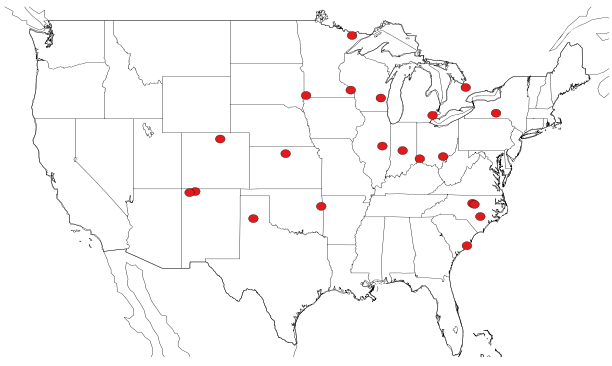

Figure 2. Monitoring site locations for the Ammonia Monitoring Network (AMoN).

[17] Model estimates of sulfate and nitrate aerosol are compared to observations from the Interagency Monitoring of Protected Visual Environments (IMPROVE) network for the year 2008 [*Malm et al*., 2004]. The IMPROVE network collects $PM_{2.5}$ particles on Teflon, nylon, and quartz filters using a modular, cyclone-based sampler with critical orifice flow control. Sulfate and nitrate aerosols are collected on nylon filters, which are sampled over 24 h every third day.

4. Inversions With Pseudo Data

[18] We first assess the capabilities and limitations of the GEOS-Chem inverse modeling setup in idealized control conditions by designing inverse problems with known solutions. A common framework for testing inverse modeling is the so-called twin experiment in which model simulations are used to generate pseudo observations [*Talagrand and P. Courtier*, 2008]. In our setup, pseudo observations are generated through application of the TES NH_3 retrieval algorithm [*Shephard et al*., 2011] to a simulated atmosphere from GEOS-Chem (i.e., radiative transfer calculations are performed to generate pseudo spectra with nominal TES instrument noise, and pseudo NH_3 retrievals produced from these). The standard model emissions used during this simulation are designated as the true emissions. Sampling times, locations, and error estimates reflect those of actual TES observations, although retrieval bias (**b**) is not included in these tests. For these tests, 87 pseudo TES observations are used from 14 to 19 July 2005, along roughly a dozen global survey transects crossing the midwestern U.S.

[19] To test the inverse model, NH_3 emissions parameters are initialized to values different from the true emissions. In the first test, initial model emissions are half of the true value. Figure 3(a) shows these values in black along with linear line slope m and R^2. After optimization, the recovered emissions are unbiased and have a visible variance around the true emissions of ~30%, as shown in blue in Figure 3(a). In a second test using the same pseudo observations, the model emissions are initially biased high by a factor of 1.8 (Figure 3(b)). The emissions recovered after optimization have a 20% high bias and again a 30% variance about the true values. While the variance of the recovered emissions is similar in both tests, the inversion starting with emissions that are initially too high is less successful.

[20] To further investigate the reasons for this asymmetry and the variance of the optimized emissions, additional tests are performed to separate the possible impacts of inversion error, retrieval bias, and measurement error. In each of the following tests, the true emissions are used to initialize the inversion. The first test uses the same pseudo observations as previously generated. This test again results in a high bias. As the same model state is used to generate the pseudo observations as was used to initialize the inversion, this bias can be attributed to a high bias in the retrieval itself. Retrieval bias, as explained further in *Shephard et al*. [2011], is owing to the fact that the retrieval always selects a moderate or polluted profile as an initial guess in order to avoid the null space of the radiative transfer operator. As the optimal estimation algorithm iterates towards a solution, the process may halt when values reach TES's detection threshold, resulting in a high bias. To test this, the retrieval algorithm is modified to use only a moderate profile as an

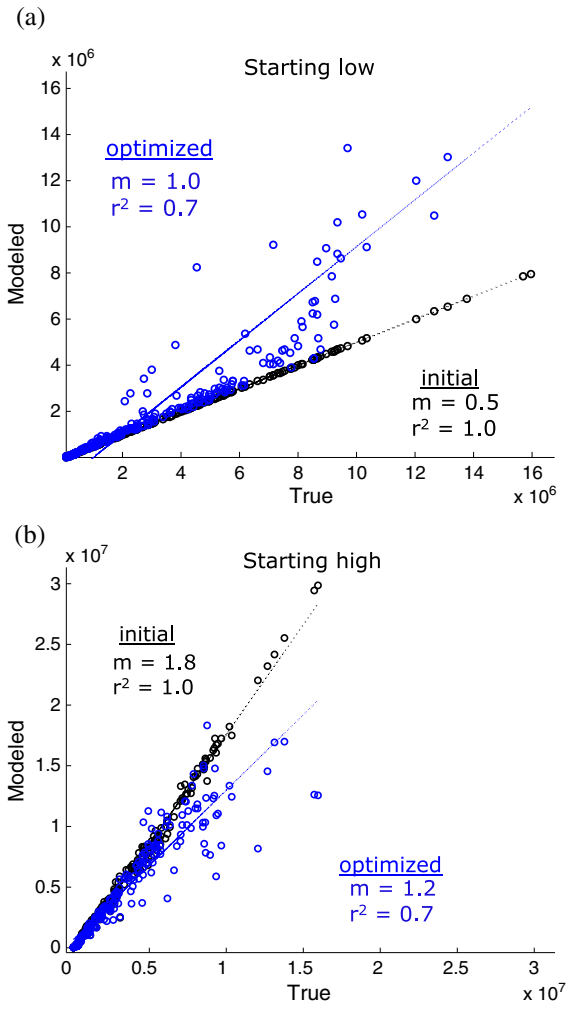

Figure 3. Emissions before (initial) and after (optimized) inversions using TES pseudo observations. To test the inverse model, NH_3 emissions were initialized to values different than the true emissions. (a) The initial emissions are half of the true values. (b) The initial emissions are 1.8 times the true values. The black points are the total initial emissions in each grid cell, and the blue points are the optimized emissions (both in kg/box).

initial guess. Pseudo observations generated using these profiles lead to slightly less high bias in the inversion, at the cost of increased variance; see Figure 4(b). As the magnitude of the final bias in tests whose results shown in Figure 4(a) and 4(b) are similar to those in the pseudo inversions, it seems that the retrieval bias explains the bias exhibited in the pseudo inversions, and thus, the entire process of inverting for NH_3 emissions is not appreciably intrinsically biased. To isolate the impact of measurement noise, the model profiles from the true model are ascribed realistic measurement error and then assimilated. These profiles, unlike the previous tests, correspond directly to the true model and are not retrieved profiles from the retrieval process. The impact of this measurement noise is only a slight adjustment in the emissions. Thus, the variance exhibited in the pseudo inversions is intrinsic to the inversion process itself and would occur even if observations were perfect. This happens

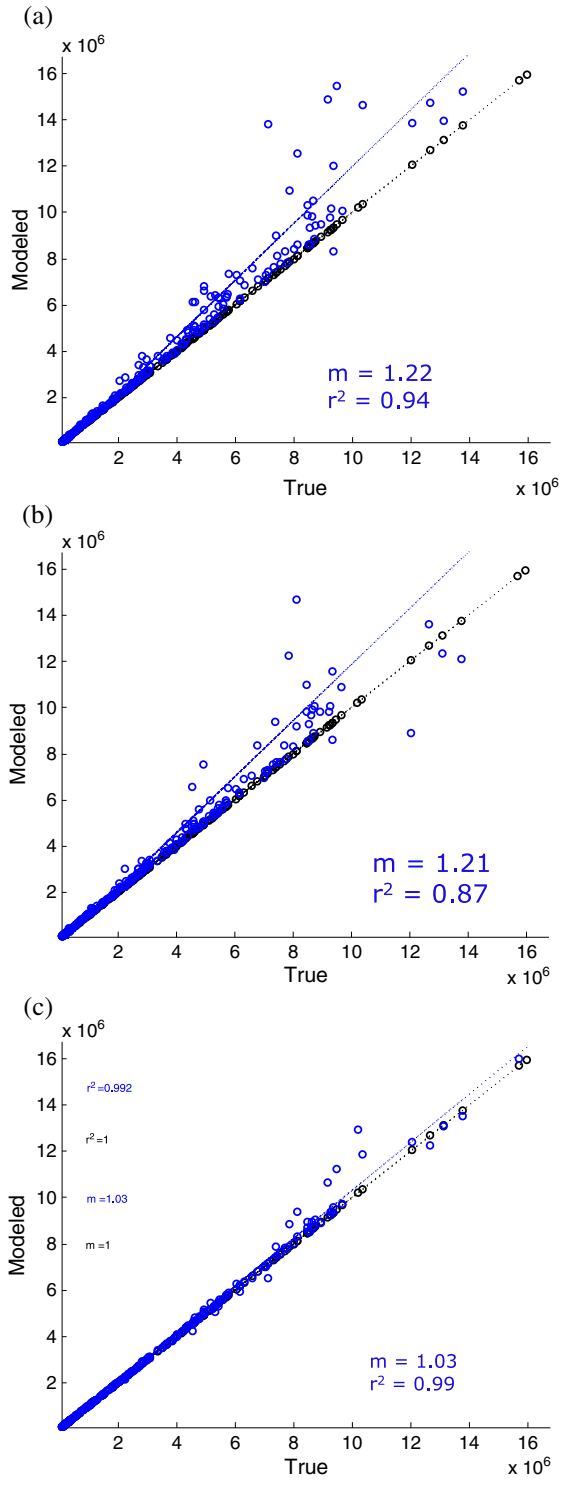

Figure 4. Tests for the possible impacts of inversion error, retrieval bias, and measurement error: (a) retrieval algorithm with a polluted profile as an initial guess; (b) modified retrieval algorithm with a moderate profile as the initial guess; (c) model profiles from the true model were ascribed error of the same size as the measurement error. The black points are the total initial emissions in each grid cell, and the blue points are the optimized emissions (both in kg/box).

because there are variations in emissions that lie in the null space of the forward model. In other words, having some emissions too high and some emissions too low can result in indistinguishable (to TES) distributions of NH_3. Overall, the pseudo observation tests lead us to conclude that (1) measurement noise alone will not lead to unstable inversions, (2) emissions that are underestimated can likely be recovered, (3) emissions that are overestimated will be decreased, though this is countered by bias in the retrievals leading to overestimate of emissions in conditions where the model emissions are initially too high, and (4) that many more iterations and observations would be necessary to reduce the variance of the emissions estimates from the truth, which will be at best ∼30%. While this variance is substantial, this is a significant improvement over initial errors of ∼100%. Contrast between points (2) and (3) is likely owing to the larger magnitude of the bias for retrievals with larger values (see Supporting Information Figure S1).

5. TES Assimilation

[21] We next proceed to constrain U.S. NH_3 sources using real observations. TES observations are compared to model estimates from a 2008 GEOS-Chem global $2° \times 2.5°$ simulation using equation (2) to assimilate individual observations. The lifetime of NH_3 is short compared to the residence time of an air mass in one grid cell of our model. As single retrievals may reflect strong sub-grid gradients in NH_3 concentration, we consider satellite observations during four years, 2006–2009, to provide enhanced spatial data coverage for comparison with the 2008 model simulations. Inter-annual comparisons of monthly AMoN NH_3 data indicate no substantial trends in this time period (Figure S3).

[22] Thousands of TES retrievals are available for the assimilation, but not all of the TES retrievals are usable. The satellite cannot always detect NH_3 for several reasons, such as the presence of clouds, low NH_3 concentrations (low signal-to-noise ratio), and poor thermal contrast between the earth and atmosphere. Thus, quality and diagnostic flags are defined to classify and filter the retrievals, keeping only those that have degree of freedom for signal (DOFS) greater than 0.1 or DOFS less than 0.1 but with high (absolute value greater than 7K) thermal contrast. We use the retrievals from daytime only as the retrievals at night are currently being further validated. The TES retrievals are corrected by subtracting mean biases. These biases are generated from the discrepancy between TES retrievals and true profiles [*Shephard et al*., 2011], and the mean biases are calculated according to the type of the a priori profile (Figure S1). There is separate bias associated with each of the three types of a priori profiles used in the retrieval algorithm. For example, we apply the "unpolluted" bias correction to all observations in which the unpolluted a priori model profile was used in the retrieval algorithm.

[23] A key aspect of inverse modeling is regularization through inclusion of the penalty, or background, term in the cost function, specified through the prior error covariance matrix, $\mathbf{S}_a$, and a regularization parameter, γ. In the absence of rigorous statistical information on the error covariances of the emissions, we assume the errors are uncorrelated and use an L-curve selection criteria [*Hansen*, 1998] (Figure S2) to regularize our solution. Still, the relative error for each species is specified as follows. Given the large discrepancies previously noted for NH_3 sources [*Henze et al*., 2009], uncertainties of NH_3 are taken to be 100% of the maximum NH_3 emissions across the globe. Based on work by other researchers, we assume that the uncertainties in SO_2 [*Lee et al*., 2011] and NO_x [e.g., *Russell et al*., 2012] are smaller, conservatively 20% and 50% of the maximum (the impact of these assumed values is assessed in Section 5 and Table 2). With these values, we select the regularization parameter (γ) to be 124 for April, 100 for July, and 50 for October.

[24] TES NH_3 observations are assimilated using the GEOS-Chem adjoint-based inversion. The domain-wide average model NH_3 profiles before and after the inversion are shown along with the average TES profile in Figure 5. The model NH_3 profiles are predominately lower than the TES observations in the prior simulation and have shifted towards the TES profile in the optimized simulation. This leads to reductions of the cost function of 66%, 42%, and 57%, for April, July, and October, respectively. The optimization is considered to have converged when consecutive iterations decrease the cost function by less than 2%. An example of the minimization is provided in Figure S4. While we recognize that further iterations are possible, for practical purposes (each iteration requiring ∼10 h to compute), this was deemed a sufficient convergence criteria. Limited tests indicate that additional iterations did not drastically alter the results.

[25] The total initial and optimized ammonia emissions are shown in Figure 6. The optimized emissions generally increase over the U.S., with adjustments that are seasonally and spatially heterogeneous. There are large increases in Southern California in all 3 months. Other large increases are located in the central and western U.S., as well as parts of Mexico and Cuba. We do not have much information about NH_3 in Mexico and Cuba due to lack of ground-based measurement records there, but large (e.g., 15 ppb) NH_3 RVMR values are observed in April whereas the corresponding GEOS-Chem model estimates using the initial emissions are very small (e.g., 1.37 ppb). As a result of the inversion, emissions are increased in such areas by up to a factor of 9. Changes to emissions in the East are generally much smaller; emissions in the Atlantic regional are generally unchanged in April and October, while they are higher in the North East in July, and even slightly lower in a few locations in the South.

[26] Figure 7 shows the comparison of NH_3 RVMR from TES and GEOS-Chem before and after the assimilation. There are between 500 and 700 RVMR values in each month including values from 4 years. A linear fit of the model values to the observations is performed in each month, before and after optimization. The slope of this line increases in each month which indicates that most of the RVMR values from GEOS-Chem increase after the optimization. However, the modeled NH_3 RVMRs at low values change only slightly after the optimization in all 3 months. We note however that these differences in RVMR do not reflect observation bias or uncertainty, which contribute to the cost function. In order to show the locations which have significant changes in RVMR, we consider spatial plots of the difference between the TES and GEOS-Chem RVMR before

Table 2. The Effects of A Priori Error Emissions ($\mathbf{S}_a$) on the Optimized Emissions of Different Species. Total Emissions Changes in the U.S. for NH_3, NO_x, and SO_2 When Using Different Values for the Diagonal of $\mathbf{S}_a^{\frac{1}{2}}$ in the Optimization. E^0 is the Initial Emissions.

	Uncertainties, $\mathbf{S}_a^{\frac{1}{2}}/\max(E^0)$			Total emissions changes		
Month	SO_2	NO_x	NH_3	ΔSO_2	ΔNO_x	ΔNH_3
April	20%	50%	100%	–11.9%	–14.69%	112.99%
	50%	50%	50%	–11.58%	–15.39%	99.95%
July	20%	50%	100%	–8.35%	–4.24%	54.80%
	50%	50%	50%	–10.23%	–4.58%	53.26%
October	20%	50%	100%	–3.56%	–1.99%	36.07%
	50%	50%	50%	–3.64%	–2.41%	35.16%

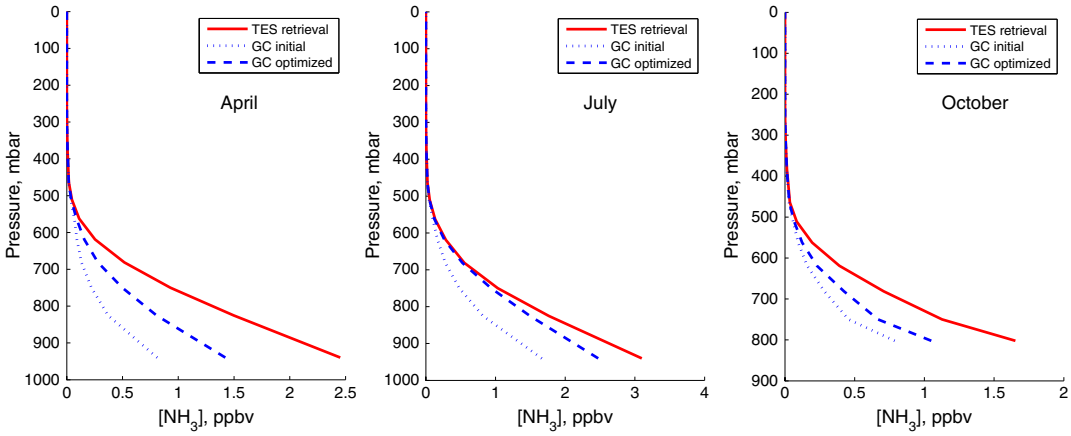

Figure 5. The average of TES retrieval profiles used in the assimilation (solid red line). The average model NH_3 profiles before (blue dotted line) and after (blue dashed line) the assimilation. The TES observation operator is applied to the model profiles.

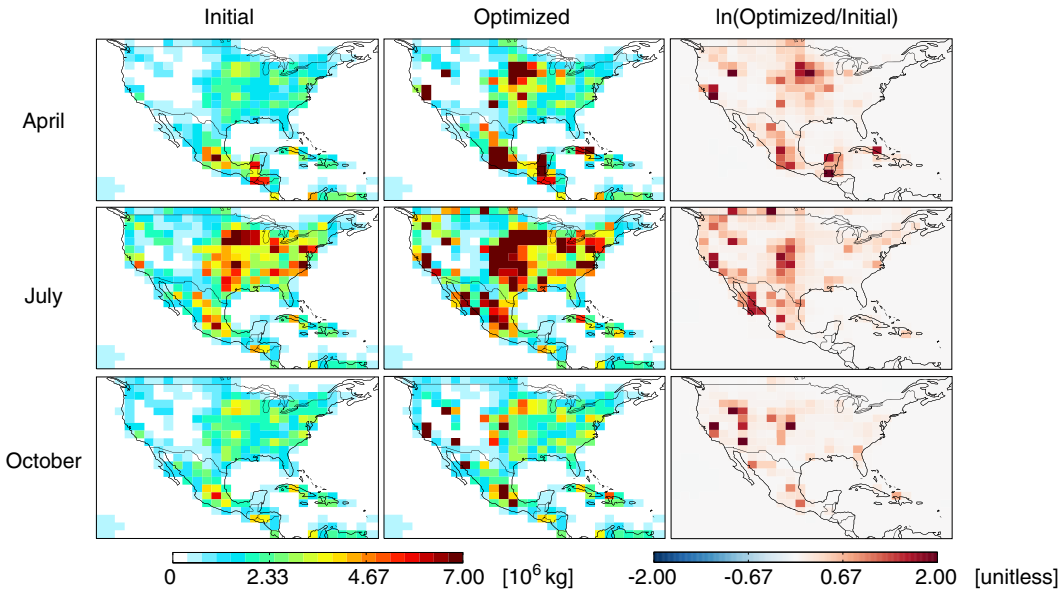

Figure 6. NH_3 emissions from GEOS-Chem before and after the assimilation.

and after the assimilation for each month (Figure 8). Initially, the model RVMRs are generally less than the TES RVMRs, as indicated by the blue points in the map. After the optimization, model RVMRs increase in many places.

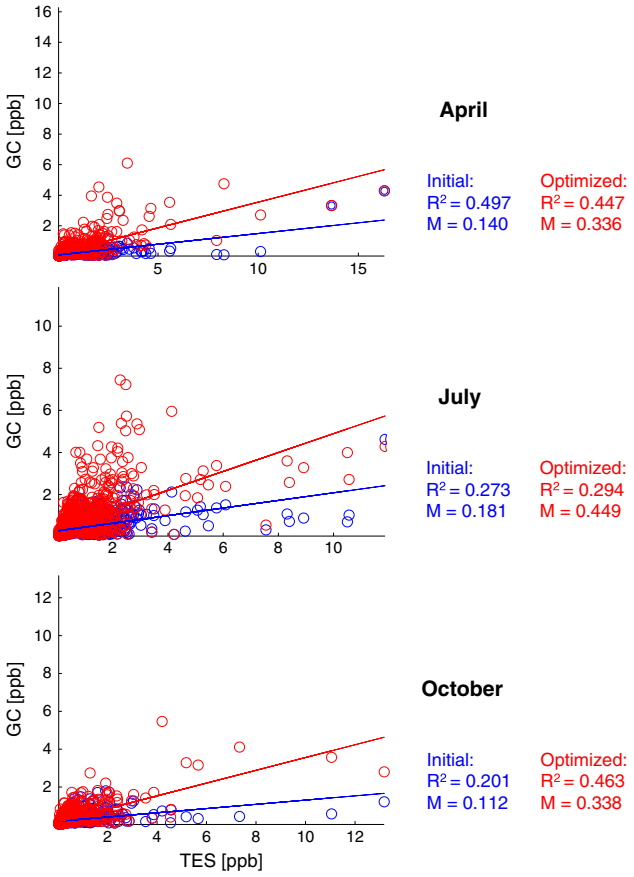

Figure 7. Comparison of NH_3 Representative Volume Mixing Ratio (RVMR) from TES and GEOS-Chem before and after the assimilation.

Some of the model RVMRs are larger than the TES RVMRs, as indicated by the red points in the map, and the overall model bias relative to TES is reduced. The discrepancies between TES RVMRs and model RVMRs change from negative to positive in Southern California and Central U.S. in all 3 months, consistent with the spatial plots showing large increases of ammonia emissions in these locations (Figure 6).

[27] We also assess the sensitivity of these results to the assumed a priori emissions errors, $\mathbf{S}_a$. Table 2 shows the effects of varying a priori errors on the total optimized emissions of different species. We assume the error for NH_3, $\mathbf{S}_a^{\frac{1}{2}}(NH_3)$, to be 50% of the maximum a priori emission for all species. Generally, the results of the inversion are not very different in terms of total emission changes for each species from the base case inversion. However, absolute changes in total emissions of SO_2 and NO_x increase slightly as their uncertainties increase relative to those of NH_3, while changes in NH_3 total emissions decrease as uncertainty of NH_3 decreases. Differences between the emissions in Table 2 compared to Table 1 stem from the use of an earlier version of the model and TES data set for performing the sensitivity calculations in Table 2; the overall findings are likely still applicable.

6. Posterior Model Evaluation Against Independent Data

[28] In the following sections, we compare output from model simulations using the optimized emissions to independent data sets not used during the inversion. This serves as an important assessment of the robustness of the inverse model solution. Even when the inverse model has converged to a solution in which the model prediction error is minimized and the emissions are consistent with the a priori error assumptions, the validity of the emissions constraints beyond this particular model framework is not guaranteed. The basic 4D-Var approach does not account for bias in the forward chemical transport model, which may significantly impact the top-down emissions constraints. Evaluating against independent data sets is thus critical.

6.1. AMoN and SEARCH

[29] We first consider a comparison of the posterior model results to AMoN NH_3 observations (Figure 9). Initially, the model broadly underestimates AMoN values. After optimization, the NH_3 concentrations increase in each month. The R^2 value increases by 22.4% in April, 29.9% in July, and 27.2% in October. The slope increases by 353.3% in April, 96.1% in July, and 77.1% in October. However, while the root mean square error (RMSE) decreases by 13% in April and 9.5% in October, it increases by 77.6% in July. The normalized mean bias (NMB) after the optimization decreases from –0.678 to –0.069 in April and increases from –0.045 and –0.138 to 0.659 and 0.166 in July and October, respectively. Overall, the model does a better job of capturing the range and variability of NH_3 at AMoN sites in April and October, while in July, the model estimates are biased high.

[30] TES has a detection limit of about 1 ppb and a positive bias of about 0.5 ppb [*Shephard et al.*, 2011]. Model values that are below 1 ppb do not change significantly after the optimization in all 3 months (Figure 9). The bias shown in Figure 9 for July is much higher than 0.5 ppb. One possible reason may be sampling bias due to the TES level of detectability and spatial sampling differences between the TES footprint and the model grid. This is assessed by analyzing NH_3 simulations from high-resolution (12 km × 12 km) Community Multi-scale Air Quality (CMAQ) model simulations. Surface level NH_3 concentrations throughout the U.S. are compared to concentrations from locations corresponding to successful TES retrievals. The mean surface NH_3 concentration of CMAQ at locations which have successful TES retrievals is about 30% larger than the mean value of that for the whole U.S. This comparison is facilitated by the fact that the TES footprint (5 km × 8 km) and CMAQ grid cells are similar in size. As shown in Figure 9, changes in large concentrations drive the optimization. A lack of TES observations constraining low values may allow for initial model values that already overestimate low NH_3 concentrations to become even higher in the optimized model, because high TES values, many of which are larger than the initial model estimate, will dominate the cost function. In future work, re-sampling the TES retrievals may be one way to decrease the sampling bias. Increasing the model resolution may also improve our ability to model

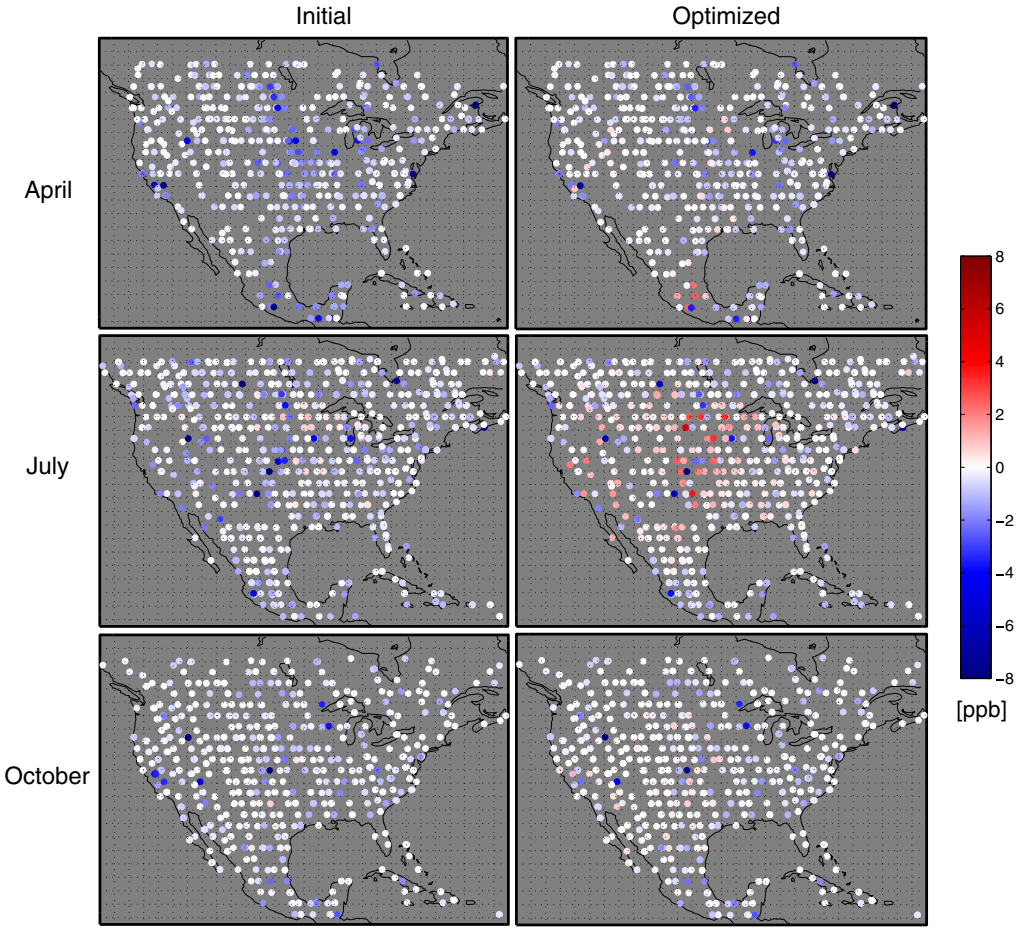

Figure 8. Difference of NH_3 Representative Volume Mixing Ratio (RVMR) between TES and GEOS-Chem before and after the assimilation. The left column shows GEOS-Chem initial RVMR-TES RVMR; the right column shows GEOS-Chem optimized RVMR-TES RVMR.

localized peak NH_3 concentrations measured by TES and to match observations from AMoN.

[31] Lastly, *Jeong et al*. [2013] also compares observations from TES and in situ NH_3 measurements to model simulations, noting similar cases where in situ measurements are lower than the model (CMAQ) simulations, but the TES observations are higher. It is suggested that treatment of the diurnal variability of summertime NH_3 emissions from livestock may play a role in this discrepancy. Comparison of GEOS-Chem hourly NH_3 concentrations to data from the SEARCH network in July paints a similar picture (Figure 10): the constant hourly NH_3 emissions in GEOS-Chem lead to NH_3 concentrations that are overestimated at night and thus also in the monthly average when compared to AMoN. Following *Jeong et al*. [2013], we perform a sensitivity calculation wherein NH_3 emissions from livestock are increased by 90% during the day and reduced by 90% at night. The impact is to decrease the monthly average surface concentrations by several ppb, while increasing daytime boundary layer NH_3 concentrations enough to reduce the cost function by 25%. In addition, *Jeong et al*. [2013] also show that bi-directional exchange of NH_3 in July leads to increased and decreased emissions in different regions (10% overall increase), yet NH_3 concentrations increase everywhere. This is in contrast to April and October, where emissions and concentrations decrease. Physical mechanisms have thus been identified by which mid-day model profiles of NH_3 may be increased without large increases in emissions. Further consideration of mechanistic, process-based treatment of NH_3 sources in global models is therefore warranted.

6.2. NTN

[32] As an additional check of the broad NH_x budget, we consider the NH_x wet deposition as recorded by NTN (NADP) sites. To make this comparison, we consider that simulated precipitation is a critical driver in the performance of the GEOS-Chem-simulated wet deposition estimates, as biases in the model estimated precipitation can lead to biases in the GEOS-Chem model estimates. We therefore adjust the modeled wet deposition diagnostic to account for differences in the modeled and observed precipitation by linearly scaling the model estimated wet deposition by the ratio of the observed to estimated precipitation.

[33] Figure 11 shows the comparison of modeled wet deposition with the NTN observations. Generally, the inversion increases wet deposition during all 3 months. Also, the square of the correlation coefficient (R^2) improves in each month: 11.4% in April, 14.1% in July, and 10.3% in October. In April and October, optimized values compare

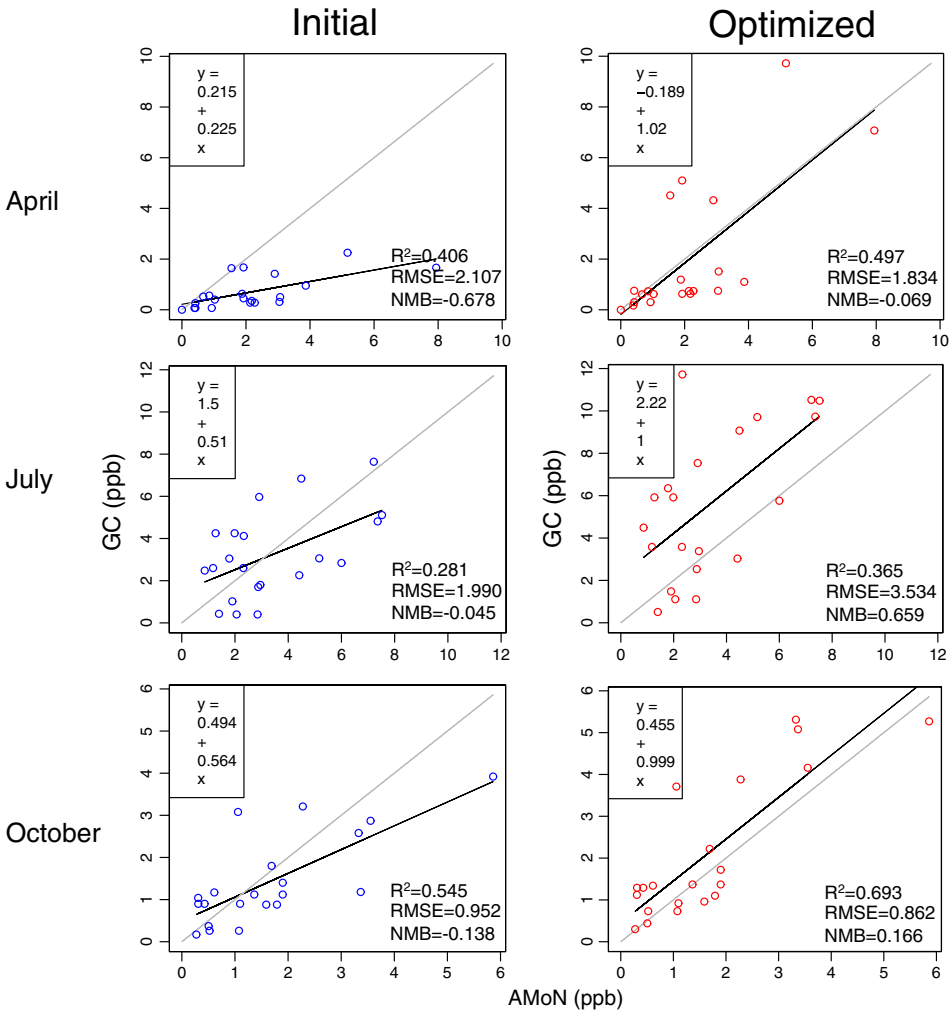

Figure 9. Comparison of GEOS-Chem NH_3 concentrations with observations from AMoN sites before and after the assimilation. The square of the correlation coefficient (R^2), root mean square error (RMSE), and normalized mean bias (NMB) are shown. Black solid lines are regressions. Gray dashed lines are 1:1.

better with the NTN observations. In contrast, the slope of the linear regression line increases from 1.08 to 1.59 in July. This is consistent with the high bias of the inversion relative to the AMoN surface observations of NH_3 in July. Comparisons between GEOS-Chem and NTN observations are also shown in *Zhang et al*. [2012]. They compare the NH_3 wet deposition from GEOS-Chem at the 0.5° × 0.67° resolution with NTN observations from 2006. Differences between this study and the present work are the model resolution, data filtering, the number of months per season included in the comparisons (one versus three), and the emission inventories in *Zhang et al*., [2012], which include domain-wide seasonal adjustments based on in situ observations to minimize seasonal bias.

6.3. IMPROVE

[34] For an additional evaluation, we also compare the assimilated results with aerosol observations from IMPROVE in 2008. Figure 12 shows that model optimization slightly decreases the sulfate concentrations and increases the nitrate concentrations, which facilitates increases in NH_3 concentrations to match TES observations. Still, the changes are small, and the sulfate concentration from the model has a reasonable correlation with the IMPROVE observation before and after optimization in each month. Note that the outlier in October that has a large observed value but a nearly zero model value is located in Hawaii. The model does not represent this high value owing to the proximity of the observation to the local volcanic source.

[35] Optimized NH_3 emissions do not help the comparison of simulated nitrate to IMPROVE observations, which initially are over predicted. The balance of sulfate and nitrate from IMPROVE sites alone implies that NH_3 sources are too high [*Henze et al*., 2009]. However, model NH_3 in the present work increases in order to improve agreement with TES NH_3, leading to more nitrate formation, and the nitrate bias becomes even higher compared to IMPROVE. It is thus a challenge to resolve the underestimates of boundary layer NH_3 with the overestimates of nitrate. HNO_3 formation in the model is perhaps excessive [*Zhang et al*., 2012], and overly shallow nighttime boundary layers may contribute to enhanced nitrate [*Heald et al*., 2012]. We perform additional sensitivity studies, reducing the heterogeneous uptake coef-

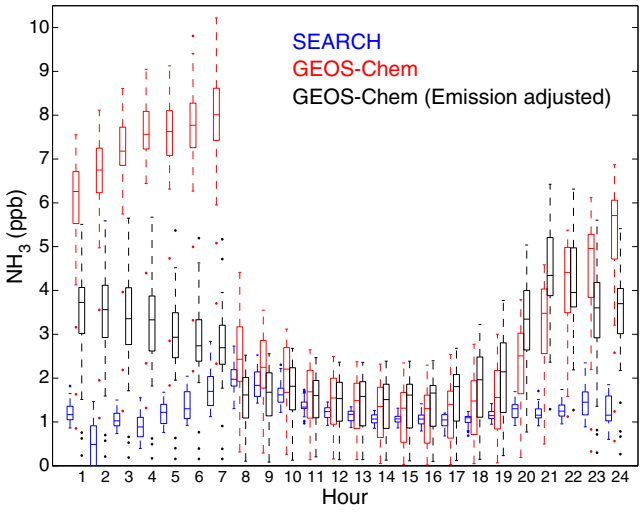

Figure 10. Comparison of initial (un-optimized) GEOS-Chem hourly NH_3 concentrations with observations from SEARCH (blue) sites in July. The red color represents the hourly NH_3 concentrations with the standard constant hourly NH_3 emissions in GEOS-Chem. The black color represents the hourly NH_3 concentrations with NH_3 livestock emissions increased by 90% during the day and reduced by 90% at night.

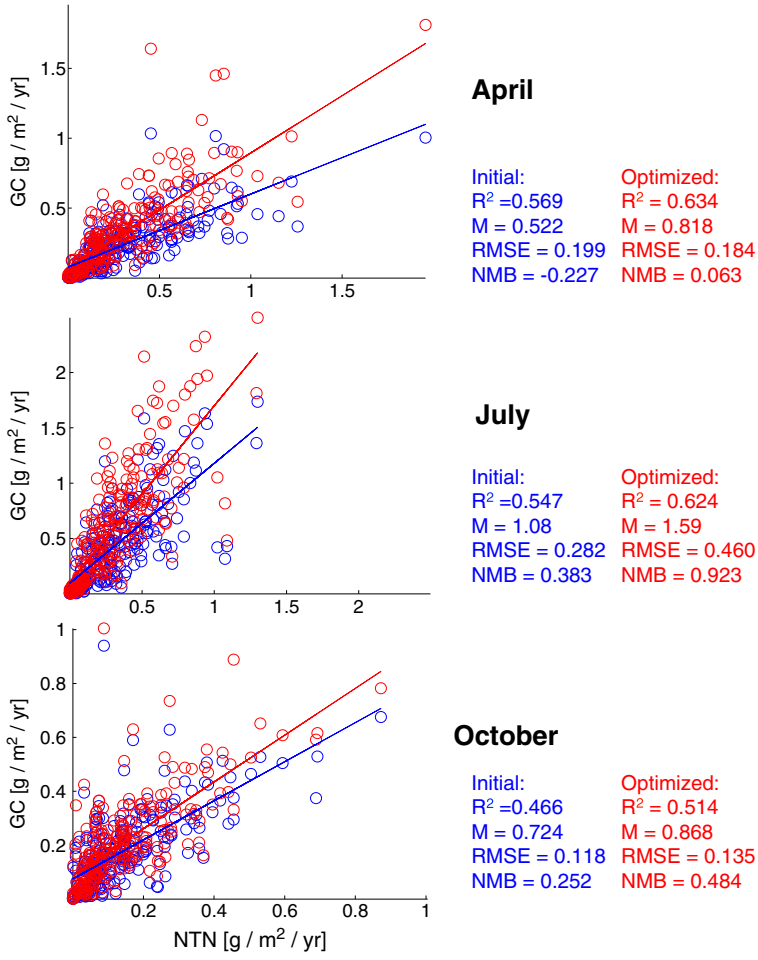

Figure 11. Comparison of GEOS-Chem NH_x wet deposition with observations from NTN (NADP) sites before (blue) and after (red) the assimilation.

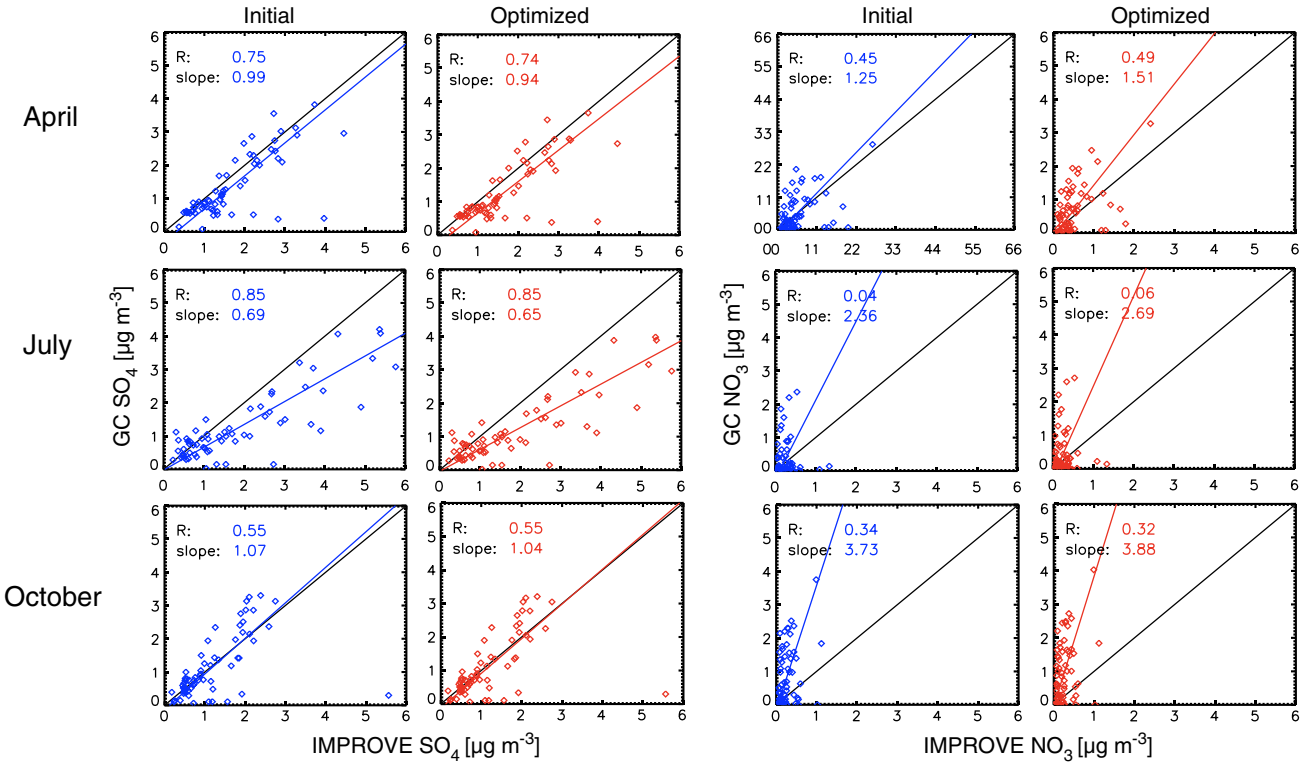

Figure 12. Comparison of GEOS-Chem SO_4 and NO_3 concentrations with observations from IMPROVE sites before and after the assimilation.

ficient for N_2O_5 hydrolysis by an order of magnitude and adjusting the boundary layer height following *Heald et al.* [2012]. While such changes do impact the nitrate simulation, the nitrate high bias persists, and the comparison of the base model NH_3 to the AMoN and TES observations was not notably affected. Enforcing a diurnal variation in NH_3 livestock emissions decreased average surface nitrate concentrations by up to a $\mu g/m^3$, as the GEOS-Chem overestimates of nighttime NH_3 likely contributed to excessive partitioning of HNO_3 at night. Thus, to achieve closure relative to all data sets, it is evident that assessment of model error beyond NH_3 sources, in terms of scavenging efficiencies, deposition, diurnal variability, and further investigation of HNO_3 production is required.

7. Conclusions

[36] Here we have considered the potential for space-based observations of NH_3 to constrain monthly average emissions. Initial tests using pseudo observations show that under ideal conditions (i.e., a perfect model) using 2 weeks worth of TES data, 70% of the variance of the emissions can be constrained in terms of total magnitude. We then proceed to assimilate TES observations in April, July, and October for multiple years. We present a range of constrained prediction results and evaluate them with independent data sets. Generally, model optimization increases NH_3 concentrations and NH_x wet deposition. Overall, the model does a better job of capturing the range and variability of NH_3 at AMoN sites in April and October, while in July, the model estimates are consistently biased high. Compared to the wet deposition observations of NTN, optimization decreases the normalized mean bias (NMB) in April, enhances the NMB in July and October, but overall leads to increased correlation of modeled and observed values. Modeled SO_4^{2-} aerosol concentrations slightly decrease, and NO_3^- aerosols concentrations increase, which increases the bias compared to the IMPROVE observations.

[37] Overall, remote sensing constraints indicate that the initial NH_3 emissions inventory appears to be broadly underestimated in several areas throughout the U.S., particularly in the West. This is consistent with recent works regarding NH_3 levels in California throughout the year [*Walker et al.*, 2012] and the U.S. in the spring [*Heald et al.*, 2012], as well as in situ measurements in April and October. Still, the absolute extent of the emissions underestimation in these seasons is still in question, as the precise accuracy of the satellite observations is difficult to specify, model resolution is not matched to the satellite resolution, and model processes could have error contributing to uncertainty in the inversion. A greater fraction of peak values are included in the assimilation owing to satellite detection limits, leading to a sampling bias that may cause the inverse model to overestimate emissions in July, as indicated by high biases in the optimized model simulations of surface level NH_3 concentrations and NH_x deposition. Future work will apply a newly developed higher resolution (e.g., 0.5° × 0.67°) version of the inverse model to further investigate this issue.

[38] Additional sensitivity studies, comparisons to hourly observations from SEARCH, and the recent regional modeling work of *Jeong et al.* [2013] indicate that diurnal variability of livestock emissions and bi-directional flux from fertilizer sources may play important roles in resolving discrepancies between average surface level concentrations

and mid-day profiles of NH_3 and may also impact the high bias of nitrate in GEOS-Chem [*Heald et al*., 2012]. Further assessment of mechanistic, process-based treatment of NH_3 sources in global models is thus needed. Additional measurements, from either expanded in situ monitoring networks or geostationary remote sensing instruments, would greatly serve this need.

[39] **Acknowledgments.** This work is supported by NASA grants NNX09AN77G and NNX10AG63G and EPA STAR award RD834559. While this manuscript has been reviewed by the Environmental Protection Agency and approved for publication, it may not reflect official agency views or policies.

References

Aneja, V. P., W. H. Schlesinger, and J. W. Erisman (2008), Farming pollution, *Nat. Geosci.*, *1*(7), 409–411, doi:10.1038/Ngeo236.

Beer, R., et al. (2008), First satellite observations of lower tropospheric ammonia and methanol, *Geophys. Res. Lett.*, *35*, L09801, doi:10.1029/2008GL033642.

Beusen, A. H. W., A. F. Bouwman, P. S. C. Heuberger, G. Van Drecht, and K. W. Van Der Hoek (2008), Bottom-up uncertainty estimates of global ammonia emissions from global agricultural production systems, *Atmos. Environ.*, *42*(24), 6067–6077, doi:10.1016/j.atmosenv.2008.03.044.

Bey, I., D. J. Jacob, R. M. Yantosca, J. A. Logan, B. D. Field, A. M. Fiore, Q. B. Li, H. G. Y. Liu, L. J. Mickley, and M. G. Schultz (2001), Global modeling of tropospheric chemistry with assimilated meteorology: Model description and evaluation, *J. Geophys. Res.-Atmos.*, *106*(D19), 23,073–23,095, doi:10.1029/2001JD000807.

Bouwman, A. F., D. S. Lee, W. A. H. Asman, F. J. Dentener, K. W. VanderHoek, and J. G. J. Olivier (1997), A global high-resolution emission inventory for ammonia, *Global Biogeochem. Cycles*, *11*, 561–587

Byrd, R. H., P. H. Lu, J. Nocedal, and C. Y. Zhu (1995), A limited memory algorithm for bound constrained optimization, *SIAM J. Sci. Comput.*, *16*(5), 1190–1208

Clarisse, L., C. Clerbaux, F. Dentener, D. Hurtmans, and P. F. Coheur (2009), Global ammonia distribution derived from infrared satellite observations, *Nat. Geosci.*, *2*(7), 479–483, doi:10.1038/Ngeo55.

Clarisse, L., M. W. Shephard, F. Dentener, D. Hurtmans, K. Cady-Pereira, F. Karagulian, M. Van Damme, C. Clerbaux, and P. F. Coheur (2010), Satellite monitoring of ammonia: A case study of the San Joaquin valley, *J. Geophys. Res.-Atmos.*, *115*, D13302, doi:10.1029/2009jd013291.

Dennis, R. L., P. V. Bhave, and R. W. Pinder (2008), Observable indicators of the sensitivity of $PM_{2.5}$ nitrate to emission reductions—Part II: Sensitivity to errors in total ammonia and total nitrate of the CMAQ-predicted non-linear effect of SO_2 emission reductions, *Atmos. Environ.*, *42*(6), 1287–1300, doi:10.1016/J.Atmosenv.2007.10.036.

Galloway, J. N., A. R. Townsend, J. W. Erisman, M. Bekunda, Z. C. Cai, J. R. Freney, L. A. Martinelli, S. P. Seitzinger, and M. A. Sutton (2008), Transformation of the nitrogen cycle: Recent trends, questions, and potential solutions, *Science*, *320* (5878), 889–892, doi:10.1126/Science.1136674.

Gilliland, A. B., R. L. Dennis, S. J. Roselle, and T. E. Pierce (2003), Seasonal NH_3 emission estimates for the Eastern United States based on ammonium wet concentrations and an inverse modeling method, *J. Geophys. Res.-Atmos.*, *108*(D15), 4477, doi:10.1029/2002JD003063.

Gilliland, A. B., K. W. Appel, R. W. Pinder, and R. L. Dennis (2006), Seasonal NH_3 emissions for the continental United States: Inverse model estimation and evaluation, *Atmos. Environ.*, *40*(26), 4986–4998, doi:10.1016/j.atmosenv.2005.12.066.

Hansen, D. A., E. S. Edgerton, B. E. Hartsell, J. J. Jansen, N. Kandasamy, G. M. Hidy, and C. L. Blanchard (2003), The southeastern aerosol research and characterization study: Part 1. Overview, *J. Air Waste Manage. Assoc.*, *53*, 1460–1471, doi:10.1080/10473289.2003.10466318.

Hansen, P. (1998), *Rank-deficient and discrete III-posed problems: Numerical aspects of linear inversion*, Society for Industrial Mathematics, PA, USA.

Heald, C. L., D. J. Jacob, R. J. Park, L. M. Russell, B. J. Huebert, J. H. Seinfeld, H. Liao, and R. J. Weber (2005), A large organic aerosol source in the free troposphere missing from current models, *Geophys. Res. Lett.*, *32*, L18809, doi:10.1029/2005GL023831.

Heald, C. L., et al. (2006), Concentrations and sources of organic carbon aerosols in the free troposphere over North America, *J. Geophys. Res.-Atmos.*, *111*(D23), D23S47, doi:10.1029/2006JD007705.

Heald, C. L., et al. (2012), Atmospheric ammonia and particulate inorganic nitrogen over the United States, *Atmos. Chem. Phys. Discuss.*, *12*, 10,295–10, 312, doi:10.5194/acp-12-10295-2012.

Henze, D. K., A. Hakami, and J. H. Seinfeld (2007), Development of the adjoint of GEOS-Chem, *Atmos. Chem. Phys.*, *7*, 2413–2433, doi:10.5194/acp-7-2413-2007.

Henze, D. K., J. H. Seinfeld, and D. Shindell (2009), Inverse modeling and mapping U.S. air quality influences of inorganic $PM_{2.5}$ precursor emissions using the adjoint of GEOS-Chem, *Atmos. Chem. Phys.*, *9*, 5877–5903, doi:10.5194/acp-9-5877-2009.

Henze, D. K., D. T. Shindell, F. Akhtar, R. J. D. Spurr, R. W. Pinder, D. Loughlin, M. Kopacz, K. Singh, and C. Shim (2012), Spatially refined aerosol direct radiative forcing efficiencies, *Environ. Sci. Technol.*, *46*, 9511–9518, doi:10.1021/es301993s.

Jeong, G.-R., et al. (2013), Evaluation of reduced nitrogen with ammonia bidirectional fluxes in CMAQ using in-situ and satellite observation, submitted.

Lee, C., R. V. Martin, A. van Donkelaar, H. Lee, R. R. Dickerson, J. C. Hains, N. Krotkov, A. Richter, K. Vinnikov, and J. J. Schwab (2011), SO_2 emissions and lifetimes: Estimates from inverse modeling using in situ and global, space-based (SCIAMACHY and OMI) observations, *J. Geophys. Res.*, *116*, D06304, doi:10.1029/2010JD014758.

Liao, H., D. K. Henze, J. H. Seinfeld, S. Wu, and L. J. Mickley (2007), Biogenic secondary organic aerosol over the United States: Comparison of climatological simulations with observations, *J. Geophys. Res.-Atmos.*, *112*, D06201, doi:10.1029/2006JD007813.

Malm, W. C., B. A. Schichtel, M. L. Pitchford, L. L. Ashbaugh, and R. A. Eldred (2004), Spatial and monthly trends in speciated fine particle concentration in the United States, *J. Geophys. Res.-Atmos.*, *109*(D3), D03306, doi:10.1029/2003jd003739.

Nowak, J. B., et al. (2006), Analysis of urban gas phase ammonia measurements from the 2002 Atlanta Aerosol Nucleation and Real-Time Characterization Experiment (ANARChE), *J. Geophys. Res.-Atmos.*, *111*(D17), D17308, doi:10.1029/2006JD007113.

Nowak, J. B., J. A. Neuman, R. Bahreini, A. M. Middlebrook, J. S. Holloway, S. A. McKeen, D. D. Parrish, T. B. Ryerson, and M. Trainer (2012), Ammonia sources in the California South Coast Air Basin and their impact on ammonium nitrate formation, *Geophys. Res. Lett.*, *39*, L07804, doi:10.1029/2012GL051197.

Park, R. J., D. Jacob, B. D. Field, R. Yantosca, and M. Chin (2004), Natural and transboundary pollution influences on sulfate-nitrate-ammonium aerosols in the United States: Implications for policy, *J. Geophys. Res.-Atmos.*, *109*, D15204, doi:10.1029/2003JD004473.

Park, R. J., D. J. Jacob, N. Kumar, and R. M. Yantosca (2006), Regional visibility statistics in the United States: Natural and transboundary pollution influences, and implications for the Regional Haze Rule, *Atmos. Environ.*, *40*(28), 5405–5423, doi:10.1016/j.atmosenv.2006.04.059.

Payne, V. H., S. A. Clough, M. W. Shephard, R. Nassar, and J. A. Logan (2009), Information-centered representation of retrievals with limited degrees of freedom for signal: Application to methane from the tropospheric emission spectrometer, *J. Geophys. Res.*, *114*, D10307, doi:10.1029/2008JD010155.

Pinder, R. W., P. J. Adams, S. N. Pandis, and A. B. Gilliland (2006), Temporally resolved ammonia emission inventories: Current estimates, evaluation tools, and measurement needs, *J. Geophys. Res.-Atmos.*, *111* (D16), D16310, doi:10.1029/2005JD006603.

Pinder, R. W., J. T. Walker, J. O. Bash, K. E. Cady-Pereira, D. K. Henze, M. Luo, G. B. Osterman, and M. W. Shephard (2011), Quantifying spatial and temporal variability in atmospheric ammonia with in situ and space-based observations, *Geophys. Res. Lett.*, *38*, L04802 , doi:10.1029/2010GL046146.

Pope, C. A., R. T. Burnett, M. J. Thun, E. E. Calle, D. Krewski, K. Ito, and G. D. Thurston (2002), Lung cancer, cardiopulmonary mortality, and long-term exposure to fine particulate air pollution, *J. Am. Med. Assoc.*, *287*(9), 1132–1141, doi:10.1001/jama.287.9.1132.

Puchalski, M. A., M. E. Sather, J. T. Walker, C. M. Lehmann, D. A. Gay, J. Mathew, and W. P. Robarge (2011), Passive ammonia monitoring in the United States: Comparing three different sampling devices, *J. Environ. Monit.*, *13*(11), 3156–3167, doi:10.1039/c1em10553a.

Pye, H. O. T., H. Liao, S. Wu, L. J. Mickley, D. J. Jacob, D. K. Henze, and J. H. Seinfeld (2009), Effets of changes in climate and emissions on future sulfate-nitrate-ammonium aerosol levels in the United States, *J. Geophys. Res.-Atmos.*, *114*, D01205, doi:10.1029/2008JD010701.

Rabalais, N. N. (2002), Nitrogen in aquatic ecosystems, *Ambio*, *31*(2), 102–112, doi:10.1639/0044-7447(2002)031[0102:NIAE]2.0.CO;2.

Reiss, R., E. L. Anderson, C. E. Cross, G. Hidy, D. Hoel, R. McClellan, and S. Moolgavkar (2007), Evidence of health impacts of sulfate- and nitrate-containing particles in ambient air, *Inhal. Toxicol.*, *19*(5), 419–449, doi:10.1080/08958370601174941.

Rodgers, C. D. (2000), *Inverse methods for atmospheric sounding*, Series on Atmospheric, Oceanic and Planetary Physics, vol. 2, World Scientific, Singapore.

Rodhe, H., F. Dentener, and M. Schulz (2002), The global distribution of acidifying wet deposition, *Environ. Sci. Technol.*, *36*(20), 4382–4388, doi:10.1021/Es020057g.

Russell, A. R., L. C. Valin, and R. C. Cohen (2012), Trends in OMI NO_2 observations over the US: Effects of emission control technology and the economic recession, *Atmos. Chem. Phys. Discuss.*, *12*, 15,419–15,452, doi:10.5194/acpd-12-15419-2012.

Sandu, A., D. N. Daescu, G. R. Carmichael, and T. F. Chai (2005), Adjoint sensitivity analysis of regional air quality models, *J. Comput. Phys.*, *204*(1), 222–252, doi:10.1016/j.jcp.2004.10.011.

Schlesinger, W. H. (2009), On the fate of anthropogenic nitrogen, *Proc. Natl. Acad. Sci. U. S. A.*, *106* (1), 203–208, doi:10.1073/Pnas.0810193105.

Schoeberl, M. R., et al. (2006), Overview of the EOS Aura mission, *IEEE Trans. Geosci. Remote Sens.*, *44* (5), 1066–1074, doi:10.1109/Tgrs.2005.861950.

Schwartz, J., F. Laden, and A. Zanobetti (2002), The concentration-response relation between $PM_{2.5}$ and daily deaths, *Environ. Health Perspect.*, *110*(10), 1025–1029

Shephard, M. W., et al. (2008), Tropospheric Emission Spectrometer nadir spectral radiance comparisons, *J. Geophys. Res.-Atmos.*, *113*(D15), D15S05, doi:10.1029/2007jd008856.

Shephard, M. W., et al. (2011), TES ammonia retrieval strategy and global observations of the spatial and seasonal variabiity of ammonia, *Atmos. Chem. Phys.*, *11*(5), 16,023–16,074, doi:10.5194/acp-11-10743-2011.

Simon, H., D. T. Allen, and A. E. Wittig (2008), Fine particulate matter emissions inventories: Comparisons of emissions estimates with observations from recent field programs, *J. Air Waste Manage. Assoc.*, *58*(2), 320–343, doi:10.3155/1047-3289.58.2.320.

Stephen, K., and V. P. Aneja (2008), Trends in agricultural ammonia emissions and ammonium concentrations in precipitation over the Southeast and Midwest United States, *Atmos. Environ.*, *42*(14), 3238–3252, doi:10.1016/j.atmosenv.2007.05.062.

Sutton, M. A., et al. (2007), Challenges in quantifying biosphere-atmosphere exchange of nitrogen species, *Environ. Pollut.*, *150* (1), 125–139, doi:10.1016/J.Envpol.2007.04.014.

Talagrand, O., and P. Courtier (2008), Variational assimilation of meteorological observations with the adjoint vorticity equation. I: Theory, *Quart. J. Roy. Meteor. Soc.*, *113*, 1311–1328, doi:10.1002/qj.49711347812.

van der Werf, G. R., J. T. Randerson, L. Giglio, J. G. Collatz, P. Kasibhatla, and A. F. Arellano (2006), Interannual variability in globalbiomass burning emissions from 1997 to 2004, *Atmos. Chem. Phys.*, *6*, 3423–3441, doi:10.5194/acp-6-3423-2006.

van Donkelaar, A., et al. (2008), Analysis of aircraft and satellite measurements from the intercontinental chemical transport experiment (INTEX-B) to quantify long-range transport of east asian sulfur to Canada, *Atmos. Chem. Phys.*, *8*, 2999–3014, doi:10.5194/acp-8-2999-2008.

Walker, J. M., S. Philip, R. V. Martin, and J. H. Seinfeld (2012), Simulation of nitrate, sulfate, and ammonium aerosols over the United States, *Atmos. Chem. Phys.*, *12*, 11,213–11,227, doi:10.5194/acp-12-11213-2012.

Wu, S.-Y., J.-L. Hu, Y. Zhang, and V. P. Aneja (2008), Modeling atmospheric transport and fate of ammonia in North Carolina—Part II: Effect of ammonia emissions on fine particulate matter formation, *Atmos. Environ.*, *42*(14), 3437–3451, doi:10.1016/j.atmosenv.2007.04.022.

Yevich, R., and J. A. Logan (2003), An assessment of biofuel use and burning of agricultural waste in the developing world, *Global Biogeochem. Cycles*, *17*(4), 1095, doi:10.1029/2002GB001952.

Yu, S. C., R. Dennis, S. Roselle, A. Nenes, J. Walker, B. Eder, K. Schere, J. Swall, and W. Robarge (2005), An assessment of the ability of three-dimensional air quality models with current thermodynamic equilibrium models to predict aerosol $NO3^{-}$, *J. Geophys. Res.-Atmos.*, *110* (D7), D07S13, doi:10.1029/2004jd004718.

Zhang, L., D. J. Jacob, E. M. Knipping, N. Kumar, J. W. Munger, C. C. Carouge, A. van Donkelaar, Y. X. Wang, and D. Chen (2012), Nitrogen deposition to the United States: distribution, sources, and processes, *Atmos. Chem. Phys. Discuss.*, *12*(1), 241–282, doi:10.5194/acpd-12-241-2012.

Zhang, Y., S.-Y. Wu, S. Krishnan, K. Wang, A. Queen, V. P. Aneja, and S. P. Arya (2008), Modeling agricultural air quality: Current status, major challenges, and outlook, *Atmos. Environ.*, *42*(14), 3218–3237, doi:10.1016/j.atmosenv.2007.01.063.

Zhu, C., R. H. Byrd, P. Lu, and J. Nocedal, (1994), L-BFGS-B: A limited memory FORTRAN code for solving bound constrained optimization problems, *Tech. Rep.*, Northwestern University.